He³ bilayers as a simple example of deconfinement

A. Benlagra and C. Pépin

Institut de Physique Théorique (IPhT), CEA, F-91191 Gif-sur-Yvette, France and CNRS, URA 2306, F-91191 Gif-sur-Yvette, France
(Received 14 October 2008; published 15 January 2009)

We consider the recent experiments on He³ bilayers [Science **317**, 1356 (2007)] showing evidence for a quantum critical point at which the first layer localizes. Using the Anderson lattice in two dimensions with the addition of a small dispersion of the f fermion, we model the system of adsorbed He³ layers. The first layer represents the f fermions at the brink of localization, while the second layer behaves as a free Fermi sea. We study the quantum critical regime of this system, evaluate the effective mass in the Fermi-liquid phase and the coherence temperature, and give a fit of the experiments and interpret its main features. Our model can serve as well as a predictive tool used for better determination of the experimental parameters.

I. INTRODUCTION

In the last 15 years, an increasing body of experimental results has revealed remarkable properties in heavy fermions close to a zero-temperature phase transition.[1–3] The standard laws governing the behavior of metallic conductors at very low temperature appeared to be violated in heavy fermions. Proximity to a quantum critical point (QCP) was early invoked to explain the experiments[3,4] but so far, this wide body of observations remains a mystery and a challenging open problem.

Recently, a new experimental setup was explored, showing signs of quantum criticality of the same nature as for heavy fermions,[5] but in a rather different system. It consists of two layers of He³ fermions adsorbed on two layers of He⁴; those themselves adsorbed on a graphite substrate. The history of He³ films adsorbed on graphite is quite rich.[6–9] A first layer of He³ has been adsorbed on graphite in two typical situations: on top of a compressed He⁴ solid of density 11.2 nm⁻² and on top of a deuterium layer of density 9.1 nm⁻². In both cases, a solidification of the top He³ layer is observed at a ratio of densities $N_1/N_{sub}=4/7$. This "magic" number corresponds to a half-filled superlattice of unit cell $\sqrt{7}\times\sqrt{7}$ (see Fig. 1) formed on top of the triangular substrate lattice.

Specific-heat measurements show that the effective mass increases by a factor of 10 in the approach of the transition. The magnetic structure of the localized phase has been extensively studied. It is believed to be a spin liquid induced by ring exchange.[10] The precise determination of this spin liquid phase, and particularly whether it is massless or massive, and whether it has some ferromagnetic component is still under debate.[11] Then a second and third He³ layers were adsorbed. The originality of the experiment[5] is that it is the first time that, when the second layer arrives at promotion, the first layer has not yet solidified. Hence there is a regime in coverage where the two first layers hybridize while layer 1 sits on the brink of localization.

Experimental details can be found in Ref. 5. We give here a rapid summary of the main findings of this work. The second layer arrives at promotion at a total coverage of $N=6.3$ nm⁻². From 6.3 to 9.2 nm⁻², a characteristic temperature T_0 is extracted, from the specific-heat measurements,

below which the fluid bilayer has Fermi-liquid properties with an enhanced quasiparticle mass. Above T_0, a Curie law is observed as if the first layer deconfines from the heavy Fermi liquid and behaves as a localized spin while the second one behaves as a Fermi liquid. It is quite difficult, however, to separate quantitatively the contribution of each layer in the heavy Fermi-liquid phase. This characteristic temperature seems to vanish at a coverage $N_{crit}=9.95$ nm⁻², the so-called "critical coverage" by the experimentalists, with a power law

$$T_{coh} \sim \delta^{1.8}, \tag{1}$$

where $\delta=|N_{crit}-N|/N_{crit}$.

The effective mass is shown to increase by a factor of 18 at $N=9.0$ nm⁻² and seems to diverge at N_{crit} with a power law

$$m/m^* \sim \delta. \tag{2}$$

Beyond N_c, the first layer is fully localized at all temperatures investigated. However, NMR studies show that at $N_I=9.2$ nm⁻² the magnetization starts to grow in a rather abrupt manner. It is not excluded that a first-order ferromagnetic transition occurs for $N \gtrsim N_I$ but an experimental evidence for it is still not conclusive. The localized phase is believed to be a spin liquid; a small "bump" in the heat capacity marks the onset of the spin liquid parameter. Ex-
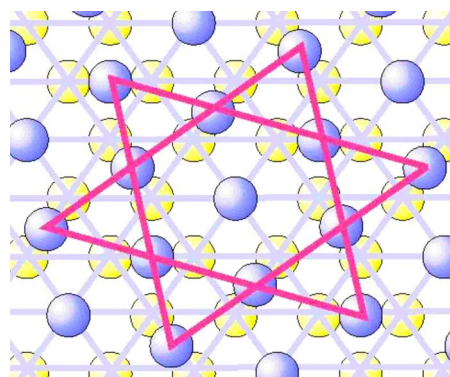

FIG. 1. (Color online) ³He solid layer on top of the triangular lattice of the substrate.

perimentally it is evaluated to be of the order of $J \sim 7$ mK. Lastly, an activation gap is extracted from the heat-capacity measurements. It decreases with increasing coverages and there are indications that it vanishes at a coverage lower than N_{crit}.

In this paper we give the details of the calculations whose results have been announced in a previous letter.[12] We apply the theory of the Kondo breakdown, previously introduced for the study of QCP in heavy fermions,[13–15] to the system of He^3 bilayers. The formalism is identical to the one developed in Ref. 14. We use the Anderson lattice model with the addition of a dispersion of the f fermions to describe the system of He^3 bilayers. The first layer, in the brink of localization, forms the lattice of f fermions. When the first layer localizes, the lattice is half-filled by construction. Strong hard-core repulsion is taken into account by a short-range Coulomb repulsion U, with $U \sim 20$ K, in agreement with the early studies of bulk He^3.[16] The top layer is modeled as a free Fermi gas. Hybridization between the two layers consists of hopping processes from layer 1 to layer 2 and vice versa.[17]

The paper is organized as follows. In Sec. II we present the Anderson lattice model and derive the slave-boson effective Lagrangian. Section III is devoted to the evaluation of the bare parameters' dependence in coverage. This is necessary if we want to confront our theory to the experimental data. We present in Sec. IV the mean-field approximation. We show the presence of a QCP at $T=0$ corresponding to the Mott localization of He^3 first layer's fermions. In particular, a peculiar behavior of the effective hybridization explains the apparent occurrence of two QCPs in the experimental data. We then study the fluctuations in Sec. V discussing the critical regime and computing the effective mass and the coherence temperature in an intermediate energy regime corresponding to a dynamical exponent $z=3$. We conclude in Sec. VII with our main result and give a criticism of our work. Some technical details are presented in the appendices. Appendix A shows the calculation of the integrals used at the mean-field approximation. In Appendix B, we give the details of the evaluation of the fermionic contribution to the corrections of scaling of the holon mass and discuss the stability of the QCP. Finally, in Appendix C, we derive an expression of the free energy starting from the Luttinger-Ward formula.

II. MODEL

Our starting point is the Anderson lattice model,

$$\mathcal{H} = \sum_{\langle i,j \rangle, \sigma} \{\widetilde{f}_{i\sigma}^\dagger [t_{ij}^0 + (E_0 - \mu)\delta_{ij}]\widetilde{f}_{j\sigma} + c_{i\sigma}^\dagger (t_{ij} - \mu\delta_{ij})c_{j\sigma}\}$$
$$+ V\sum_{i\sigma} (\widetilde{f}_{i\sigma}^\dagger c_{i\sigma} + \text{H.c.}) + \sum_i (U\widetilde{n}_{f,i}^2 + U_1\widetilde{n}_{f,i}n_{c,i}), \quad (3)$$

where $\langle i,j \rangle$ refers to nearest-neighbor sites created by the graphite's corrugate potential, σ is a spin index, $\widetilde{f}_{i\sigma}^\dagger(\widetilde{f}_{i\sigma})$ are creation (annihilation) operators for the first layer's fermions, and $c_{i\sigma}^\dagger(c_{i\sigma})$ are creation (annihilation) operators for the second layer's fermions. $t_{ij} = t$ is the c-fermion's hopping, t_{ij}^0

$= \alpha t$ is the f-fermion's hopping term, V is the hybridization between the two layers, E_0 is the energy level of the f fermions, and μ is the chemical potential. $\widetilde{n}_{f,i} = \Sigma_\sigma \widetilde{f}_{i\sigma}^\dagger \widetilde{f}_{i\sigma}$ and $n_{c,i} = \Sigma_\sigma c_{i\sigma}^\dagger c_{i\sigma}$ are the operators describing the particle number of each layer's fermions. U and U_1 are, respectively, the intra- and interlayer Coulomb repulsions. The model is studied in the limit of very large on-site repulsion U. We expect to have a coverage dependent hopping parameter $t \equiv t(N)$ as well as hybridization $V(N)$. Furthermore, we have $U1 \ll U$, but we keep the interlayer interaction term for now.

Superexchange terms can be generated by a second-order expansion in large $U/(\alpha t)$ and $U_1/(\alpha t)$. The Hamiltonian is then written as

$$\mathcal{H} = \sum_{\langle i,j \rangle, \sigma} \{\widetilde{f}_{i\sigma}^\dagger [t^0 + (E_0 - \mu)\delta_{ij}]\widetilde{f}_{j\sigma} + c_{i\sigma}^\dagger (t - \mu\delta_{ij})c_{j\sigma}\}$$
$$+ V\sum_{i\sigma} (\widetilde{f}_{i\sigma}^\dagger c_{i\sigma} + \text{H.c.}) + \sum_{\langle i,j \rangle} J(\widetilde{\mathbf{S}}_{f,i} \cdot \widetilde{\mathbf{S}}_{f,j} - \widetilde{n}_i\widetilde{n}_j/4)$$
$$+ J_1 \widetilde{\mathbf{S}}_{f,i} \cdot \mathbf{S}_{c,j}, \quad (4)$$

where $J = 2(\alpha t)^2/U$, $J_1 = 2(\alpha t)^2/U_1$, and $\widetilde{\mathbf{S}}_f = \Sigma_{\alpha,\beta} f_\alpha^\dagger \sigma_{\alpha\beta} f_\beta$ is the spin operator with $\vec{\sigma}$ the Pauli matrix. RKKY interaction, mediated by the conduction electrons, as well as various ring exchange parameters studied in Ref. 18 can be included in the J term.

One key approximation of this work is that we consider that at the edge of localization, the f fermions are half-filled. This means that the f fermion somehow forms their "own" lattice as the coverage increases, so that when the localization occurs, we are at half-filling. This approximation is necessary if we want to attribute the observed increase of the effective mass to strong correlations coming from Mott physics. However, we do not have a microscopic justification for it; only the coherence of the findings of this approach can justify it. The on-site Coulomb repulsion U is very large (~ 20 K), leading to strong correlation effects. In the limit $U \rightarrow \infty$, there is a constraint of no double occupancy which we account for using Coleman's slave boson,[19] decoupling the f-fermion's creation operator at each site "i" as

$$\widetilde{f}_{i\sigma}^\dagger \rightarrow f_{i\sigma}^\dagger b_i, \quad (5)$$

where $f^\dagger$, the creation operator of the so-called "spinons," and $b^\dagger$, the one of the holons, obey the local constraint $\Sigma_\sigma f_{i\sigma}^\dagger f_{i\sigma} + b_i^\dagger b_i = 1$. Upon the transformation (5), the slave boson drops of all bilinear products of fields at the same site.

The constraint is taken into account in a Lagrangian formulation through a Lagrange multiplier λ. The effective Lagrangian is then

$$\mathcal{L} = \sum_{\langle i,j \rangle, \sigma} \{f_{i\sigma}^\dagger [(\partial_\tau + \epsilon_{f,i})\delta_{ij} + b_i t^0 b_j^\dagger]\widetilde{f}_{j\sigma} + c_{i\sigma}^\dagger [(\partial_\tau - \mu)\delta_{ij}$$
$$+ t]c_{j\sigma}\} + \sum_i b_i^\dagger (\partial_\tau + \lambda_i)b_i - \lambda_i + V\sum_{i\sigma} (f_{i\sigma}^\dagger b_i c_{i\sigma} + \text{H.c.})$$
$$+ \sum_{\langle i,j \rangle} J(\mathbf{S}_{f,i} \cdot \mathbf{S}_{f,j} - n_i n_j/4) + J_1 \mathbf{S}_{f,i} \cdot \mathbf{S}_{c,j}, \quad (6)$$
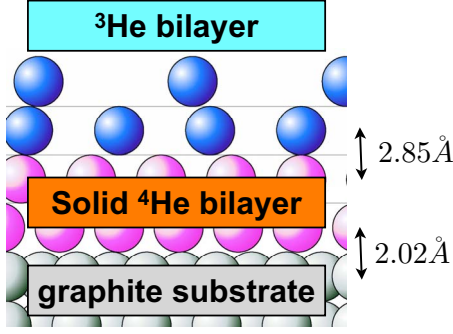
FIG. 2. (Color online) ³He solid layers on top of the triangular lattice of the substrate; we show here the various heights of the layers one compared to the other.

where $\epsilon_{f,i} = E_0 - \mu + \lambda_i$ is the renormalized f-band's chemical potential.

The short-range magnetic interaction and the induced Kondo interaction are decoupled using Hubbard-Stratanovich transformations $J\mathbf{S}_{f,i} \cdot \mathbf{S}_{f,j} \rightarrow \phi_{i,j} f_{i\sigma}^\dagger f_{j\sigma} - |\phi_{ij}|^2/J$ and $J_1\mathbf{S}_{f,i} \cdot \mathbf{S}_{c,j} \rightarrow \sigma_i f_{i\sigma}^\dagger c_{i\sigma} - |\sigma_i|^2/J_1$.

The Lagrangian becomes now

$$\mathcal{L} = \sum_{\langle i,j\rangle,\sigma} \{f_{i\sigma}^\dagger [(\partial_\tau + \epsilon_{f,i})\delta_{ij} + b_i t^0 b_j^\dagger + \phi_{ij}]\widetilde{f}_{j\sigma} + c_{i\sigma}^\dagger [(\partial_\tau - \mu)\delta_{ij}$$
$$+ t]c_{j\sigma}\} + \sum_i b_i^\dagger (\partial_\tau + \lambda_i)b_i + \sum_{i\sigma} [f_{i\sigma}^\dagger (Vb_i + \sigma_i)c_{i\sigma} + \text{H.c.}]$$
$$- \sum_i [\lambda_i + |\sigma_i|^2/(J_1)] - \sum_{\langle i,j\rangle} |\phi_{ij}|^2/J. \tag{7}$$

We assume that ϕ_{ij} condenses in a uniform spin liquid phase, i.e., $\langle \phi_{ij}\rangle = \phi_0$. It renormalizes the dispersion of the spinon band and ensures the breakdown of the Kondo effect.[13] It is shown to stay roughly constant through the phase diagram $\phi_0 = \beta t \approx J$.[14] σ_i merely renormalizes the effective hybridization Vb_i.

III. PARAMETERS

Before going further, we need to evaluate the dependence of the bare parameters in coverage in order to fit the experimental data. The height of the layers is taken from the study by Roger *et al.*[18] The first ⁴He layer's height is ≈ 2.02 Å while the other one's height is ≈ 2.85 Å (see Fig. 2). From the experiment,[5] the density of He⁴ layers is 9.2 nm⁻² while the one of the first He³ layer is $N_1 = 6.3$ nm⁻².

The total coverage is defined as

$$N = N_c + N_f,$$

$$N_f = N_1(1 - n_b), \tag{8}$$

where N_f and N_c are, respectively, the coverages (in nm⁻²) of the first and second layers and n_b is the number of holons per site. At the transition, we have

$$N_f/N_1 = 1, \tag{9}$$

which accounts for the fact that at the transition, the f fermions are in a 1/2 filled lattice. This means that the number of

holons n_b vanishes at the QCP. Away from the QCP, the number of holons is allowed to fluctuate freely and its value is determined self-consistently. The parameter J is extracted from the experiment:[5] $J = 7$ mK.

The evaluation of the bandwidth, $D = 2t = \pi/m$, for each layer of He³ is based on an analysis of Pricaupenko and Treiner[20] where the kinetic energy of liquid He³ contains a density-dependent effective mass

$$\frac{\hbar^2}{2m^*} = \frac{\hbar^2}{2m}\left(1 - \frac{\bar{\rho}}{\rho_c}\right)^2, \tag{10}$$

where $\bar{\rho} = 3/(4h_c)n(\text{Å}^{-2})$ is the average density inside a sphere of radius $h_c = 2.63$ Å and $\rho_c = 0.04$ Å⁻³.

We have then

$$D_f = D(1 - 0.07N_f)^2,$$

$$D_c = D[1 - 0.07(N - N_f)]^2,$$

where D is the bandwidth of ³He in the bulk.

At half filling, $N_f = N_1$, the mean kinetic energy $E_{\text{kin},f}$ equals the bandwidth D_f. We have

$$E_{\text{kin},f} = \frac{\hbar^2}{2m_f^* N_1} \int_0^{k_F} \frac{d^2\mathbf{k}}{(2\pi)^2} k^2,$$

$$= \frac{\hbar^2 \pi^3}{16m_f^*} N_1, \tag{11}$$

where $k_F = \pi/\sqrt{N_1}$ ($\sqrt{N_1}/2$ is the average radius of a particle in the first layer).

We find then at half-filling

$$E_{c,f} \approx 0.52 \text{ K},$$

$$D_f = 0.30D,$$

$$D_c = 0.62D,$$

thus, $D \approx 1.73$ K, $D_f \approx 0.57$ K, and $D_c \approx 1.18$ K, which gives a value $\alpha = 0.54$ for the ratio between the bandwidths. This value is relatively high compared to the typical values for rare-earth compounds for which $\alpha \equiv 0.1$.

A word has to be said at this stage. We have considered the spherical dispersion of the free fermions

$$\epsilon_\mathbf{k} = \frac{k^2}{2m} - \frac{k_F^2}{2m},$$

for which the density of states (DOS), defined by $\frac{d^2k}{4\pi^2} = \rho(\epsilon)d\epsilon$, is constant

$$\rho(\epsilon) = \frac{m}{2\pi}.$$

However, as emphasized in Sec. I, the first layer solidifies into a triangular lattice. For a triangular lattice tight-banding band structure, the dispersion is given by

$$\epsilon_\mathbf{k} = -2t[\cos(k_x) + 2\cos(k_x/2)\cos(\sqrt{3}k_y/2)].$$

(a)   (b)
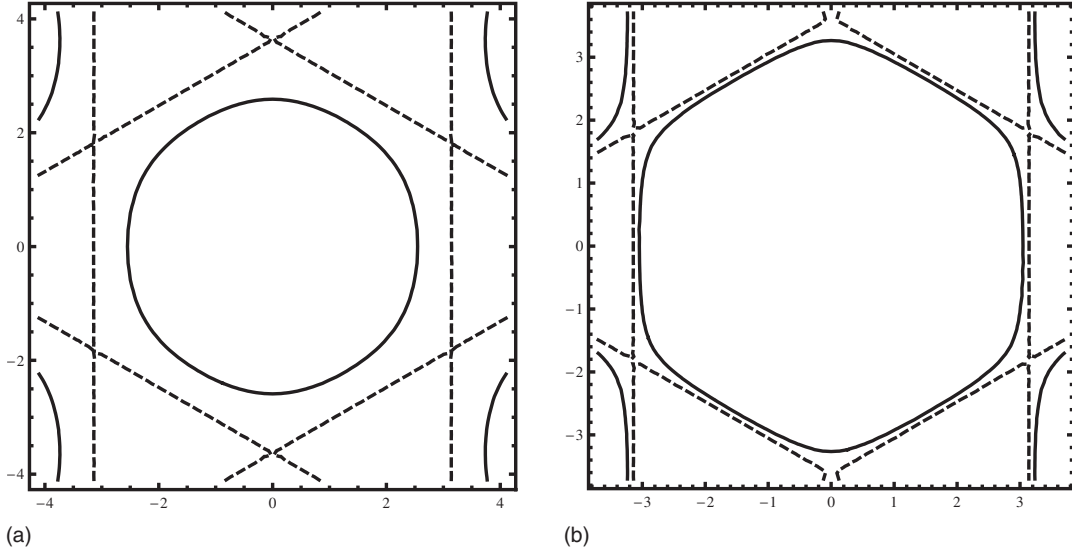
FIG. 3. The Fermi surface at unit coverage (a) $\delta=0.10$ and (b) $\delta=0.15$. We see that the Fermi surface in the former is still circular while it experiences, for the second one, small deviation from the circular case.

The Fermi surface for fermions in a triangular lattice is no longer circular at each filling, but we can consider that these deviations are benign in the range of coverage studied in our case, in particular very close to the QCP.

Figure 3 shows the Fermi surface of the f fermions at two different coverages: (a) $\delta=0.10$ for which $D_f\approx0.52$ K, $\epsilon_f\approx0.13$ K and (b) $\delta=0.15$ for which $D_f\approx0.60$ K, $\epsilon_f\approx0.54$ K. In the latter case, the Fermi surface deviates around the circular Fermi surface for free fermions. The approximation of constant DOS can still hold and this can be seen indeed by considering the DOS profile for the triangular lattice case shown in Fig. 4. The hatched region marks the energy scales of our model, and we see that we are far from the Van Hove singularity, and we can approximate the DOS by a constant one.

The chemical potential μ is defined by the filling of the second layer

$$\frac{N_c}{6.3} = \int_{D_c}^{\mu} \rho_0 d\epsilon.$$
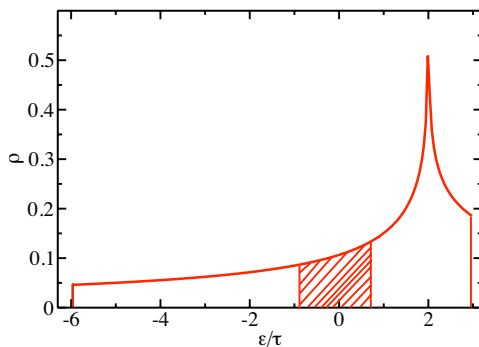
We get directly

FIG. 4. (Color online) Density of states for a triangular lattice tight-banding structure. Characteristic energy scales in our model lie within the hatched region.

$$\mu = D_c\left(\frac{2N_c}{6.3} - 1\right). \tag{12}$$

E_0 is identified as the difference between the potential energies of the two layers.[21] Each layer experiences two kinds of interactions:

(1) Van der Waals interaction with the grafoil substrate

$$V_s(z) = (4C_3^3/27D^2)1/z^9 - C_3/z^3, \tag{13}$$

where $D=192$ K is the well depth of the potential and $C_3=2092$ K Å^3 is the Van der Waals constant,[20] and

(2) the Bernardes-Lennard Jones interaction between two He particles

$$V_{LJ}(z) = 4\epsilon[(\sigma/r)^{12} - (\sigma/r)^6], \tag{14}$$

with $\epsilon=10.2$ K and $\sigma=2.56$ Å is the hard-core radius.[18] Thus, for the layer L_i, the potential energy writes

$$E_{f,c} = V_s(z_i) + v_i, \tag{15}$$

with

$$v_i = \pi\sum_j \rho_j \int rdr V_{LJ}(r), \tag{16}$$

where ρ_j is the density of each layer and "j" is the layer's index. The chemical potential E_0 now reads

$$E_0 = E_f - E_c. \tag{17}$$

We denote (see Fig. 2) r_1, r_2, r_3, and r_4, respectively, the distances of the first, second, third, and fourth layers to the graphite center. We have

$$z_1 = 2.2 \text{ Å}, \quad z_2 = 5.03 \text{ Å}, \quad z_3 = 7.9 \text{ Å}, \quad z_4 = 10.57 \text{ Å}. \tag{18}$$

Applying Eq. (13) we get $V_s(z_3)=-4.21$ K and $V_s(z_4)=-1.77$ K. These orders of magnitude are quite big compared to the typical scale of a few millikelvins for this sys-

tem. Its order of magnitude is in accordance with Ref. 18.

We turn now to the Lennard-Jones potential. We sum up Eq. (14) for all two-body interaction in all the layers. We get for the first layer or f fermions

$$v_f = \pi \left[\rho_1 \int_{r_m^1}^\infty r dr V_{LJ}(r) + \rho_2 \int_{r_m^2}^\infty r dr V_{LJ}(r) \right. $$
$$\left. + \rho_3 \int_{r_m^3}^\infty r dr V_{LJ}(r) + \rho_4 \int_{r_m^4}^\infty r dr V_{LJ}(r) \right], \quad (19)$$

with

$$\rho_1 = 0.092, \quad \rho_2 = 0.092,$$

$$r_m^1 = 5.7, \quad r_m^2 = 2.85,$$

$$\rho_3 = 10^{-2} N_1(1 - n_b), \quad \rho_4 = 10^{-2}[N - N_1(1 - n_b)],$$
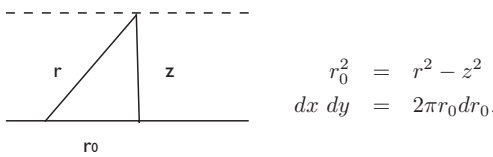
$$r_m^3 = \rho_3^{-1/2}, \quad r_m^4 = 2.85.$$

For the second layer or c fermions, we get

$$v_c = \pi \left[\rho_1 \int_{r_m^1}^\infty r dr V_{LJ}(r) + \rho_2 \int_{r_m^2}^\infty r dr V_{LJ}(r) \right. $$
$$\left. + \rho_3 \int_{r_m^3}^\infty r dr V_{LJ}(r) + \rho_4 \int_{r_m^4}^\infty r dr V_{LJ}(r) \right], \quad (20)$$

with

$$\rho_1 = 0.092, \quad \rho_2 = 0.092,$$

$$r_m^1 = 8.55, \quad r_m^2 = 5.7,$$

$$\rho_3 = 10^{-2} N_1(1 - n_b), \quad \rho_4 = 10^{-2}[N - N_1(1 - n_b)],$$

$$r_m^3 = 2.85, \quad r_m^4 = \rho_4^{-1/2}.$$

The values of r_m^j are now in angstrom,

$$r_0^2 = r^2 - z^2$$
$$dx\,dy = 2\pi r_0 dr_0.$$

We finally get

$$v_f = -3.87 - 1.08N - 6.75n_b + I_3, \quad (21)$$

with

$$I_3 = -0.196(1 - n_b)^3 [11.2 - 0.3(1 - n_b)^3],$$

and

$$v_c = -7.69 + 6.75n_b + J_4 \quad (22)$$

with

$$J_4 = -\pi 10^{-2}[N - 6.25(1 - n_b)^3]$$
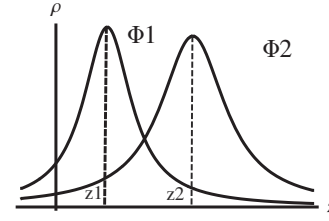$$\times \{0.29 - 3.2 10^{-5}[N - 6.25(1 - n_b)^3]\}.$$

E_0 now reads

FIG. 5. Sketch of layers' density profile. The hybridization is estimated from the overlap between the wave functions of the two layers.

$$E_0 \equiv 1.65 - 1.071N - 10^{-6}N^2 - 13.5n_b - 2.25(1 - n_b)^3$$
$$+ 0.059(1 - n_b)^6. \quad (23)$$

The last parameter and the most crucial in fact is the hybridization V. It is defined as the hopping strength between the two layers. We can have an estimate of V using Eq. (10) to get the same dependence as in Eq. (11)

$$V = V_0[1 - 0.07(N - N_f)](1 - 0.07N_f).$$

Here, V_0 is proportional to the overlap between the ground-state wave functions of the two layers, i.e.,

$$t_{12} \approx \delta V \int dz \Phi_1(z) \Phi_2(z),$$

where Φ_i^k is the ground-state wave function of layer i and $\delta V = V_s(z_4) - V_s(z_3)$.

The latter is taken as a Slater determinant of single-particle states Φ_i^k which writes, assuming translational invariance parallel to the surface,[18,22]

$$\Phi_i^k(\mathbf{r}) = \frac{1}{2\pi} \phi_i^k(z) \exp[i(k_x x + k_y y)].$$

Density functional models show a Lorentzian-type profile (Fig. 5) for the density of each layer along the z direction[20]

$$\rho_i \equiv |\phi_i(z)|^2 = \frac{b_i}{(z - z_i)^2 + a_i^2}.$$

From Ref. 18 we have

$$\text{for } L_1: a = 1.7, \quad b = 0.115,$$

$$\text{for } L_2: a = 3.42, \quad b = 0.32.$$

We find then $V_0 \approx 0.6$ K, consistent with the value obtained in a previous study.[21]

As said before, the hybridization V is actually a crucial parameter. Indeed, the mean-field value for the QCP reads $J/t = \exp[E_0 D_c / V^2]$.[13,14] We see then that any small variation in the dependence of V on coverage has an exponential impact on the position of the QCP. We consider V thus as a fitting parameter that will tune the position of the QCP.

We have taken

$$V = V_0[1 - 0.07(N - N_f)](1 - 0.07N_f) + V_1\delta + V_2\delta^2,$$

where V_0, V_1, and V_2 are adjusted to fit the experimental data and $\delta = (N_{crit} - N)/N_{crit}$. We used $V_0 = 1.55$ K, $V_1 = 15.9$ K, and $V_2 = -4.5$ K.
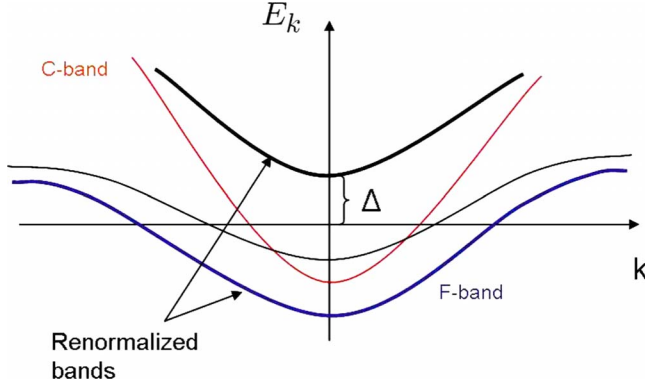
FIG. 6. (Color online) Sketch of the different dispersions: the lower band (blue line) is the dispersion of the spinons and the upper (bold black line) band is the dispersion of the conduction electrons. The Kondo gap Δ is defined as the difference between the chemical potential and the upper band.

IV. MEAN-FIELD THEORY

At the mean-field level, we make a uniform and static approximation for the holon field and the Lagrange multiplier. The free energy then writes

$$F_{\mathrm{MF}} = -2T\sum_{k,\sigma,\omega_n,\pm} \ln[-G_{\pm}^{-1}(i\omega_n,\mathbf{k})] + \lambda(b^2 - 1),$$

(24)

where ω_n is the fermionic Matsubara frequency and $G_{\pm}^{-1} = i\omega_n - E_{\mathbf{k}\pm}$, with

$$E_{\mathbf{k}\pm} = \frac{1}{2}[\epsilon_{\mathbf{k}} + \epsilon_{\mathbf{k}}^0 \pm \sqrt{(\epsilon_{\mathbf{k}} - \epsilon_{\mathbf{k}}^0)^2 + 4V^2b^2}].$$

In the above, $\epsilon_{\mathbf{k}}$ is the dispersion of the conduction electrons, $\epsilon_{\mathbf{k}}^0 = (\alpha b^2 + \beta)\epsilon_{\mathbf{k}} + \epsilon_f$ is the spinon dispersion, and $E_{\mathbf{k}\pm}$ the dispersion of the renormalized upper $(+)$ and lower $(-)$ bands (see Fig. 6) The former derives from the c fermions with weak f character whereas the latter derives from the f fermions with weak c character.

Minimizing Eq. (24) with respect to the holon field b and the Lagrange multiplier λ, one gets the following mean-field equations:

$$T\sum_{k,\sigma,\omega_n} (\alpha\epsilon_{\mathbf{k}}G_{ff} + VG_{fc}) + \epsilon_f - E_0 = 0,$$

$$T\sum_{k,\sigma,\omega_n} G_{ff} + b^2 = 1,$$

(25)

where

$$G_{ff} = \frac{i\omega_n - \epsilon_{\mathbf{k}}^0}{(i\omega_n - E_{\mathbf{k}+})(i\omega_n - E_{\mathbf{k}-})},$$

$$G_{fc} = \frac{Vb}{(i\omega_n - E_{\mathbf{k}+})(i\omega_n - E_{\mathbf{k}-})} \equiv VbP_{fc}.$$

(26)

These equations are solved in the case of a linearized dispersion bandwidth at zero temperature $(T=0)$. The summation over $(\mathbf{k}, \omega_n)$ is performed analytically and is given in Appen-
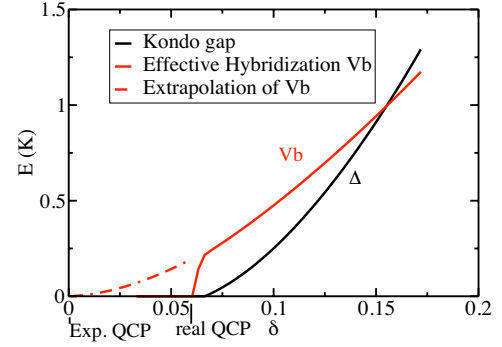

FIG. 7. (Color online) Mean-field phase diagram for the Anderson lattice model in $D=2$ applied to He^3 bilayers (Ref. 23). Following Ref. 5, $\delta = 1 - N/N_{\mathrm{crit}}$ with $N_{\mathrm{crit}} = 9.95$ nm^{-2}. The effective hybridization (red line) drops suddenly at $\delta \approx 0.063$, indicating the real QCP. The experimental QCP is obtained by extrapolation of Vb to zero ($E=0$). The Kondo gap Δ (black line) vanishes before the real QCP Ref. 12.

dix A. The set of resulting equations is then solved numerically.

Figure 7 shows the plot of the order parameter, defined as the effective hybridization Vb, and the "Kondo gap" Δ, defined as the energy difference between the chemical potential and the upper band (see Fig. 6), as a function of $\delta = 1 - N/N_{\mathrm{crit}}$.

In our model, the Kondo gap is identified with the activation energy observed experimentally in the specific heat. We have two bands in the model: one for the spinons and one for the conduction electrons. At very low hybridization, when the bands just start to hybridize, there is no energy difference between the lower and the upper bands. As the hybridization grows, the upper band becomes empty and an activation gap opens. We see on Fig. 7 that the gap closes at the very vicinity of the QCP.

The set of mean-field equations shows a QCP where $b \to 0$, the so-called Kondo breakdown (KB) QCP,[13,14,24] which implies that the spinons experience a Mott transition and their band is half-filled. We observe that Vb goes to zero, before the experimentally observed QCP occurs, at a unit coverage $\delta \approx 0.063$. This constitutes one main finding of this paper. The localization occurs before the experimental QCP is reached. Our interpretation is that first, the experimental QCP is evaluated by extrapolating to zero temperature the power laws for the effective mass and the coherence temperature. Second, a key feature of the model is that the hybridization is strong compared to the other parameters (it is of the order of the bandwidth), hence the falling down of the order parameter close to the transition is very abrupt.

This fact is illustrated in Fig. 7 where we see that the order parameter's behavior has two regimes: it starts to grow very quickly at the QCP then reaches, at the "elbow," a regime of strong hybridization. The behavior of the order parameter is governed by the relative strength of the bare hybridization V compared to the other energies of the model. The former is already big at the QCP, $V_c \approx 1.63$ K, thus the slope of the effective hybridization is steep in the hybridized phase. The sharp change corresponds to the emptying of the upper band, the same point at which the opening of the
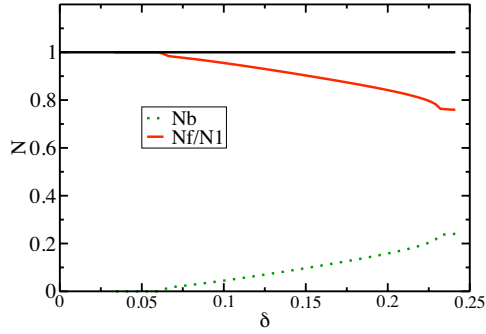
FIG. 8. (Color online) The number of bosons n_b (green dashed line) and of the f fermions (red line) per site in the system as well as their sum (black line). The local constraint of no double occupancy is preserved throughout the explored coverage range.

Kondo gap occurs. This point is situated after the real QCP in the hybridized phase because when the localization occurs, the f band is half-filled and the upper band is constrained to sit below the chemical potential and is thus occupied. The vanishing of the Kondo gap before the QCP is observed experimentally if we identify it as the activation gap extracted from the thermodynamic measurements of Neumann *et al.*[5] We can make the same construction as the experimentalists by extrapolating the order parameter in the high energy regime to zero temperature. We find an additional QCP that we identify with the "experimental" one. This gives an explanation of the mysterious presence of two QCPs in this system; the magnetization starts to grow at the physical QCP before the experimental one is reached. Indeed, as soon as the first layer localizes, one expects the static magnetic susceptibility to grow quickly since the spin liquid parameter is small $J \sim 7$ mK. Note that the distance in coverage between the two QCPs is in agreement with the experimental data.

In Fig. 8 we have plotted directly the number of holons in the hybridized phase, as given from our mean-field theory. The number of holons determines the number of holes in the first layer as compared to the value at half-filling. We can see that although the order of magnitude is correct close to the QCP, far away from it we obtain some values of n_b too big from what is observed experimentally. In particular, it is believed that close to the coverage corresponding to the promotion of the second layer, the number of holons should decrease so that the number of f fermions in the first layer should be again close to half-filling. We do not observe any hint of this decreasing. It shows that the domain of validity of our model is close to the QCP. Far away from it, we miss the physics of exhaustion,[25,26] where there are not enough free fermions in the second layer to Kondo screen the many f fermions in the first layer.

V. FLUCTUATIONS

In what follows we will be interested in fitting the experimental data. We identify the regime of critical fluctuations experimentally accessible with the higher energy regime of the order parameter (see Fig. 7). Within our theory, we are
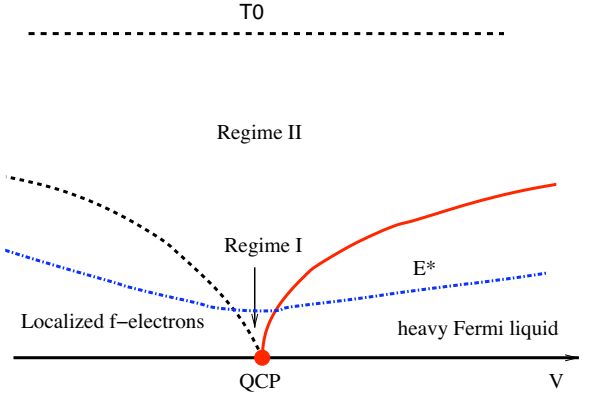

FIG. 9. (Color online) Schematic for the Kondo breakdown QCP in the Anderson lattice (Ref. 14) On the left, where the holons are not condensed, is the localized phase. On the right is the heavy Fermi phase. The QCP is multiscale; for $T \leq E^*$, the dynamical exponent is $z=2$ and for $T \geq E^*$ it is $z=3$.

situated in the intermediate regime around the Kondo breakdown QCP, i.e., the regime for which the dynamical exponent $z=3$. We refer the reader to previous studies of the Kondo breakdown for more details.[13–15,27] To give a small summary of the situation (see Fig. 9), the main finding of the Kondo breakdown QCP is its multiscale character. There exists an energy scale E^* differentiating two regimes. In the low-temperature regime we have the dynamical exponent z $=2$ (Ref. 28) with no damping. In the high-temperature regime, we have the exponent $z=3$ and the bosonic mode corresponding to the fluctuations of the order parameter is overdamped by the particle-hole continuum. In this paper we focus on the $z=3$ regime, arguing that E^* is very small in this system.

Indeed, from the theory (see, for example, Ref. 27) we know that $E^* \simeq 0.1(q^*/q)^3 T_K$, with q^* the mismatch of the two Fermi surfaces at the QCP. Here T_K can be taken as the typical energy scale of the system which is typically of the order of $T_K = 100$ mK. At the QCP, we evaluate q^*/k_F which is

$$q^*/k_F = 1 - k_c/k_F,$$

$$= 1 - (6.3/9.95)^{1/2},$$

$$= 0.2.$$

Hence we obtain

$$E^* = 8.10^{-4} T_K,$$

$$= 8.10^{-5} \text{ K}, \tag{27}$$

which is a too small energy scale to be accessible experimentally for this setup.

The holon propagator in the intermediate regime ($z=3$) reads

$$D_b^{-1}(q,\Omega_n) = D_0^{-1}\left[q^2 + \xi^{-2} + \frac{\gamma|\Omega_n|}{\alpha' q}\right], \quad (28)$$

with $D_0 = 4k_F^2/(\rho_0 V^2)$, $\gamma = mV^2 D_0/(\pi v_F)$, $\alpha' = b^2\alpha + J/t$, $\rho_0 = m_c/(2\pi)$ is the c fermions density of states, and ξ is the correlation length, associated with the fluctuations of b, given by $\xi^2 = D_0^{-1}m_b^{-1}$, where m_b is the holon mass at $T=0$.
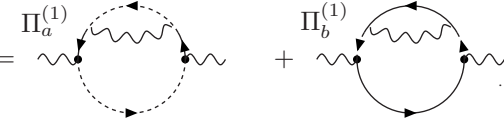
A. Holon mass

The static part of the holon mass is evaluated by differentiating twice the mean-field energy (24) with respect to the holon field b given the constraints (25). One finds

$$m_b = 2bT\sum_{\mathbf{k},\omega}\left[\alpha\epsilon_{\mathbf{k}}\frac{\partial G_{ff}}{\partial b} + V^2\frac{\partial P_{fc}}{\partial b}\right]. \quad (29)$$
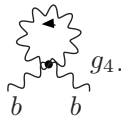
The summation over $(\mathbf{k},\omega)$ is evaluated analytically for a linearized dispersion bandwidth at $T=0$ and the result is given in Appendix A.

The temperature dependence of the holon mass is computed by evaluating the corrections to scaling to the boson propagator. There are two types of corrections to scaling. One contribution is the renormalization of the boson propagator coming to their coupling to the fermion loops
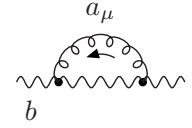

This type contribution was first evaluated close to a QCP in Ref. 29. We first note that the two diagrams are proportional: $\Pi_a^{(1)} = \alpha'\Pi_b^{(1)}$ and that there is no corresponding vertex insertion at the first order. Hence, although the QCP occurs in the charge channel, we have no cancellation of this set of diagrams. This is in deep contrast to what occurs close to a ferromagnetic QCP or in the theory of nonanalytic corrections to the Landau Fermi liquid, where this set of diagrams cancels in the charge channel.[30] This type of diagram is known to be dangerous and carries a minus sign, which destabilizes the fixed point. The diagram for $\Pi_a^{(1)}$ is computed in the intermediate energy regime with the dynamical exponent $z=3$.

On the other hand, we have the direct mass renormalization coming from the standard ϕ^4-type corrections to scaling, which has the opposite effect of stabilizing the fixed point

Here g_4 comes from the quartic term of the holon action derived from Eq. (24) in a Ginzburg-Landau approach and contains the ferromagnetic short-range correlations J; we find $g_4 = -J/4 + V^4/(2\alpha'^2 D^3)$. We have as well as the correction to the boson mass coming from the gauge fluctuation, which stabilizes as well the QCP, but is subdominant compared to the two previous ones

Summing the dominant diagrams (see Appendix B) yields a logarithmic correction to scaling

$$m_b(T) = m_b(T=0) + CT\log T, \quad (30)$$

where C had to be adjusted to $C = 7.5\times10^{-3}$ to fit the data, while the analytic evaluation gives

$$C = \left[\frac{(1+\alpha')}{8} - \frac{1}{3}\right]\frac{V^2}{8(\alpha' D)^2} + \frac{DJ}{6V^2}.$$

The balance of the two contributions in favor of the g_4 coupling ensures the stability of the fixed point.

B. Effective mass

The effective mass m^* is determined from the free energy of the system by

$$F = -\frac{\pi T^2}{6}m^*.$$

The free energy is evaluated using the Luttinger-Ward functional[30]

$$F = F_{\text{MF}} + T/2\sum_n\int d^2q/(2\pi)^2\log[D^{-1}(q,\Omega_n)], \quad (31)$$

where F_{MF} is the free energy at the mean field (24) and $D(q,\Omega_n)$ is the full propagator of the holons. Note that we have neglected the role of the gauge fields in this formulation because the renormalization of the effective mass is to be evaluated inside the ordered phase where the gauge fields are gapped through the Higgs mechanism. At the mean-field level, the system consists of the upper and lower bands; we get then

$$F = -\frac{\pi T^2}{6}\left[2\pi(\rho_+ + \rho_-) + \frac{\gamma\xi}{4\alpha'}\right], \quad (32)$$

where $\rho_+(\rho_-)$ is the density of states at the Fermi surface of the upper (lower) band given by

$$\rho_\pm = \rho_0\left(\frac{\partial E_{\mathbf{k}\pm}}{\partial\epsilon_{\mathbf{k}}}\right)^{-1}_{|E_\pm = 0}.$$

The calculation is done in Appendix C. The effective mass reads directly

$$m^* = 2\pi(\rho_+ + \rho_-) + \frac{\gamma\xi}{4\alpha'}.$$

The result for m^* is shown in Fig. 10 where it is compared to the results of the experiment.[5] We see that the inverse effective mass follows the same behavior as the order parameter and vanishes at the theoretical QCP. Here again, if we extrapolate the high energy regime down to zero temperature, we can identify a fictitious point where the effective
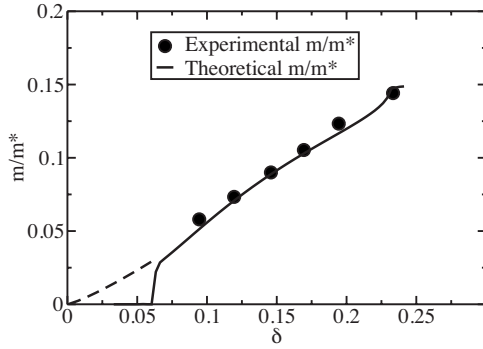
FIG. 10. The inverse effective mass m/m^* in the Anderson lattice model for the He³ bilayers. The dots are experimental data from Ref. 5. The fitting parameters for this model are detailed in the text (Ref. 12).

mass could vanish, if it has not its peculiar behavior into two regimes. This extrapolation is linear and follows closely the one found by the experimentalists.

C. Coherence temperature

The coherence temperature is defined by the crossover condition

$$m_b(T_{\mathrm{coh}}) = 0,$$

where $m_b(T)$ is the temperature-dependent holon mass given in Eq. (30). The equation is solved numerically using the results found for the order parameter b in Sec. IV and the result is plotted in Fig. 11.

The coherence temperature has the same qualitative behavior: it vanishes at the real QCP and we can extrapolate its high energy regime down to zero temperature closely to a quadratic power law in unit coverage δ. In fact, the exponents of the effective mass and the coherence temperature can be understood in a simple way. For $z=3$ theories in the Fermi-liquid phase, the effective mass goes like the correlation length[31] $m/m^* \sim \xi^{-1}$. From the dispersion of the boson mode we see that $\xi^{-1} \sim \sqrt{m_b} \sim b$. Now the coherence temperature goes like b^2. In the regime where b varies linearly with the coverage n we thus get

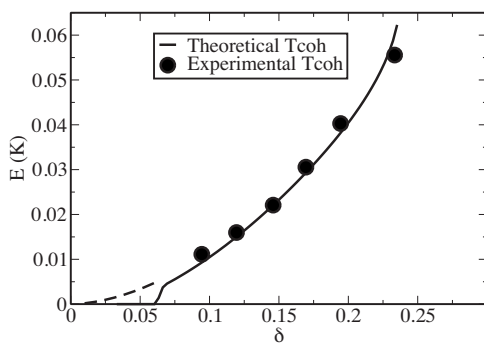$$m/m^* \sim cst - n, \quad T_{\mathrm{coh}} \sim (cst - n)^2. \tag{33}$$

FIG. 11. The coherence temperature T_{coh} in the Anderson lattice model for the He³ bilayers. The dots are experimental data from Ref. 5. The fitting parameters for this model are detailed in the text (Ref. 12).
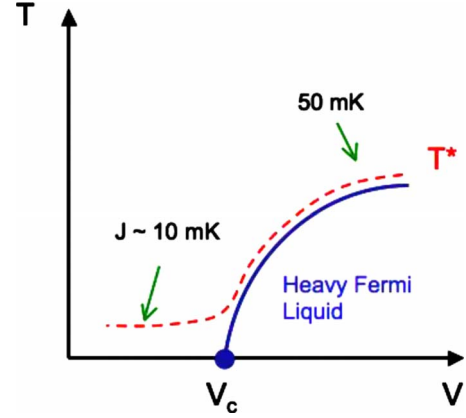

FIG. 12. (Color online) Asymmetry of the phase diagram. Above T^* the entropy $R \ln 2$ is released. There are two ways of quenching the entropy: first through the formation of the heavy Fermi-liquid phase where the hybridization is nonzero (on the right of the phase diagram) and second through the formation of the spin liquid (on the left of the phase diagram).

VI. DISCUSSION

One of the main general observation one gets from the experimental data is the asymmetry of the phase diagram as far as the quantum fluctuations are concerned. Indeed the increase of the effective mass appears only from the right of the phase diagram which corresponds to low doping (see Fig. 10). From the left of the phase diagram the fluctuations seem to be frozen out.

Another observation is the quasiabsence of quantum critical (QC) regime in temperature for this system unlike for the heavy fermions. Indeed a Curie law for the spin susceptibility is observed at very low temperatures in the localized phase and directly above T_{coh} in the hybridized phase, indicating that the system very quickly goes into a regime of free spins, hence missing the usual quantum critical regime typical of QCP. The key to understanding these two observations is that in this system the energy scales are completely different from the ones that appear in heavy fermion systems.

The Curie law is observed when the entropy $R \ln 2$ is released above a characteristic temperature T^*. In our model, two mechanisms are responsible for quenching the entropy, namely, the formation of the spin liquid and of the heavy Fermi liquid. T^* is thus determined by the relative strength of these two mechanisms. Technically, T^* is by the first irrelevant operator of the theory. We see in Fig. 12 that on the left side of the phase diagram, the main quenching mechanism corresponds to the formation of the spin liquid, while on the right side of the phase diagram, the two mechanisms coincide and are roughly of the same strength. The asymmetry of the phase diagram can thus be accounted for, in this model, by the fact that on the localized side (left side) the spinons' bandwidth, which determines the scale of the formation of the spin liquid, is typically given by the value of the exchange parameter $J \simeq 7$ mK. Alternatively, in the hybridized phase, the bandwidth of the spinons is enlarged due to the holon fluctuations $D_f = J + n_b \alpha D$. This increase of the bandwidth in the hybridized phase is typical of a slave-boson description of a Mott transition.[32]
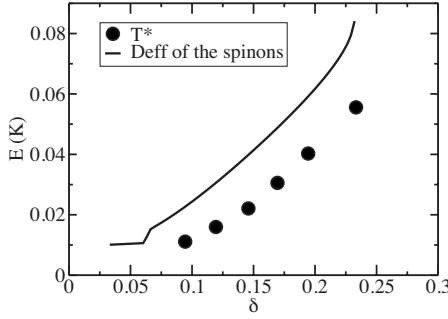
FIG. 13. The effective bandwidth of the spinons $D_f = J + \alpha D n_b$ and the experimental characteristic temperature T_0.

In the hybridized phase the coincidence, within the experimental uncertainties (between 5 and 10 mK),[5] in energy between the crossover coherence temperature and the effective bandwidth of the spinons (see Fig. 13) explains that the quantum critical regime is quenched; the free spin behavior being admittedly quickly observed above the temperature which delimits the upper-critical regime.

VII. CONCLUSIONS

In the present article, we give the details of calculation whose results have been presented in a previous letter.[12] The system studied, He^3 bilayers, is one of the simplest physical ones, with negligible spin-orbit interaction and no crystal-field interactions, to show QC similar to the one observed in complicated intermetallic heavy fermions compounds.

Using the Kondo-breakdown[13–15] scenario of an itinerant QCP, we examine the possible origin of the QC observed experimentally as fluctuations of an effective hybridization. The theoretical model is an extended version of the Anderson lattice model with a dispersion of the f fermions and inter- and intra-Coulomb repulsions.

We benefited from the extensive literature on He^3 to extract carefully most of the parameters of the model from the bare parameters. Crucial parameters, such as the hybridization, were used as fitting parameters owing to the level of approximation of our study. Finally, we have emphasized some differences with intermetallic heavy fermion compounds.

We were successful enough to account for most of the experimental features. First, we have explained why there are seemingly two apparent QCPs which fit at the right respective coverage. The experimental one results from an extrapolation to zero temperature of an intermediate energy regime, while the theoretical one characterizes the vanishing of the effective hybridization. We reproduced then the slopes *and* exponents of the coherence temperature and effective mass closely to the experimental results. The apparent lack of quantum critical behavior in temperature is qualitatively explained by the remarkably low energy scale of the spin liquid parameter on the ordered side and the coincidence between the coherence temperature and the effective bandwidth of the spinons in the hybridized one. Finally, we recover the fact that the activation gap, observed experimentally, has to vanish in the Fermi-liquid phase before the critical coverage is reached right when the system enters a strong hybridization regime for which the upper hybridized band becomes empty.

Our study suffers though from some weakness and drawbacks. We used four fitting parameters, three for the hybridization and one for the slope of the coherence temperature. This is expected in any mean-field approach, in particular owing to the crucial role of the hybridization for the Kondo breakdown QCP and cannot be avoided at this level. The fact that the number of holons n_b is too big away from the QCP, especially near the promotion coverage of the second layer, restricts the domain of validity of our model very close to the QCP. Finally, magnetism on the ordered side of the phase diagram is not handled in our model. Magnetism is best considered in the so-called slave fermions approach, which in turn describes badly the hybridized phase. But still the model is simple and strong enough to make predictions and put them to the test.

APPENDIX A: EVALUATION OF SOME INTEGRALS

In here, we will evaluate the integrals in the mean-field Eq. (25). At $T=0$, the calculation of these integrals is analytical for linearized bands in which case

$$\sum_k \rightarrow \rho_0 \int_{-D}^{D} d\epsilon, \tag{A1}$$

where ρ_0 is the density of states at the Fermi surface.

Let us call

$$\mathcal{A} = T \sum_{\mathbf{k},\sigma,\omega_n} G_{ff}(\mathbf{k}, i\omega_n),$$

$$\mathcal{B} = T \sum_{\mathbf{k}\sigma,\omega_n} P_{fc}(\mathbf{k}, i\omega_n),$$

$$\mathcal{C} = T \sum_{\mathbf{k},\sigma,\omega_n} \epsilon_{\mathbf{k}} G_{ff}(\mathbf{k}, i\omega_n),$$

$$\mathcal{D} = T \sum_{\mathbf{k},\sigma,\omega} \alpha \epsilon_{\mathbf{k}} \frac{\partial G_{ff}}{\partial b},$$

$$\mathcal{E} = T \sum_{\mathbf{k},\sigma,\omega} \frac{\partial P_{fc}}{\partial b}.$$

We diagonalize the 2×2 matrix which accounts for the hybridization of the f and c bands

$$E_{\mathbf{k}\pm} = \frac{1}{2}[\epsilon_{\mathbf{k}}^0 + \epsilon_{\mathbf{k}} \pm \sqrt{\Delta}],$$

$$\Delta = (\epsilon_{\mathbf{k}}^0 - \epsilon_{\mathbf{k}})^2 + 4(bV)^2.$$

The integrals are all performed in the same way: first by summing over the Matsubara frequencies and second by doing the momentum integration. The momentum integration is done by linearization of the band,

$$\mathcal{A} = 2T \sum_{k,\omega_n} \frac{(i\omega_n - \epsilon_\mathbf{k})}{(i\omega_n - E_{\mathbf{k}-})(i\omega_n - E_{\mathbf{k}+})}$$

$$= 2\rho_0 \int_{-D}^{D} d\epsilon \int \frac{-n_F(z)}{2i\pi} \frac{(z-\epsilon)}{(z-E_-)(z-E_+)} dz,$$

where the contour is on the whole complex plane,

$$= 2\rho_0 \int_{-D}^{D} d\epsilon \left(\frac{n_F(E_-)(E_- - \epsilon_k)}{(E_- - E_+)} - \frac{n_F(E_+)(E_+ - \epsilon_k)}{(E_- - E_+)} \right)$$

$$= \rho_0 \int_{-D}^{\epsilon_m} d\epsilon \frac{-y + \sqrt{y^2 + 4(bV)^2}}{\sqrt{y^2 + 4(bV)^2}}$$

$$- \rho_0 \int_{-D}^{\epsilon_p} d\epsilon \frac{-y - \sqrt{y^2 + 4(bV)^2}}{\sqrt{y^2 + 4(bV)^2}},$$

with ϵ_m and ϵ_p the Fermi levels for the upper and lower bands, respectively,

$$\epsilon_m = (-\epsilon_f + \alpha'\mu - \sqrt{(\epsilon_f + \alpha'\mu)^2 + 4\alpha'(bV)^2})/(2\alpha'),$$

$$\epsilon_p = (-\epsilon_f + \alpha'\mu + \sqrt{(\epsilon_f + \alpha'\mu)^2 + 4\alpha'(bV)^2})/(2\alpha'),$$

with the conditions $-D \le \epsilon_m \le 0$; $0 \le \epsilon_p \le D$ and $\alpha' = \alpha b^2 + \phi_0/D$.

One obtains

$$\mathcal{A} = \frac{\rho_0}{(1-\alpha')} [-2y_{-D} + y_m - \sqrt{y_m^2 + 4(bV)^2} + y_p$$

$$+ \sqrt{y_p^2 + 4(bV)^2}],$$

$$y_m = (1-\alpha')\epsilon_m - \epsilon_f - \mu,$$

where

$$y_p = (1-\alpha')\epsilon_p - \epsilon_f - \mu,$$

$$y_{-D} = -(1-\alpha')D - \epsilon_f - \mu.$$

We proceed in the same way for $\mathcal{B}$, $\mathcal{C}$, $\mathcal{D}$, and $\mathcal{E}$ to find

$$\mathcal{B} = \frac{2\rho_0}{(1-\alpha')} \ln \left[\frac{y_m + \sqrt{y_m^2 + 4(bV)^2}}{y_p + \sqrt{y_p^2 + 4(bV)^2}} \right],$$
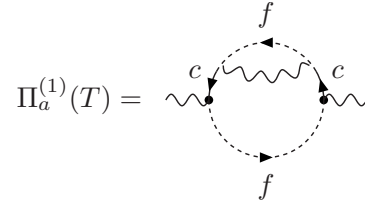
$$\mathcal{C} = \frac{\rho_0}{(1-\alpha')^2} \left[-2(\epsilon_f + \mu)(y_{-D}) + y_{-D}^2 \right.$$

$$+ 2(bV)^2 \ln \left(\frac{y_m + \sqrt{y_m^2 + 4(bV)^2}}{y_p + \sqrt{y_p^2 + 4(bV)^2}} \right) + (\epsilon_f + \mu)y_m$$

$$+ y_m^2 - (y_m/2 + \epsilon_f + \mu)\sqrt{y_m^2 + 4(bV)^2} + (\epsilon_f + \mu)y_p$$

$$\left. + y_p^2 + (y_p/2 + \epsilon_f + \mu)\sqrt{y_p^2 + 4(bV)^2} \right],$$

$$\mathcal{D} = -\frac{4\alpha V^2 b\rho_0}{(1-\alpha')^2} \ln \left[\frac{y_m + \sqrt{y_m^2 + 4(bV)^2}}{y_p + \sqrt{y_p^2 + 4(bV)^2}} \right],$$

$$\mathcal{E} = \frac{4V^2 b\rho_0}{(1-\alpha')} \left[\frac{y_p}{2V^2 b^2 \sqrt{y_b^2 + 4V^2 b^2}} - \frac{y_m}{2V^2 b^2 \sqrt{y_m^2 + 4V^2 b^2}} \right.$$

$$+ \frac{-2}{(y_m - \sqrt{y_m^2 + 4V^2 b^2})\sqrt{y_m^2 + 4V^2 b^2}}$$

$$\left. + \frac{-2}{(-y_p - \sqrt{y_p^2 + 4V^2 b^2})\sqrt{y_p^2 + 4V^2 b^2}} \right].$$

APPENDIX B: CORRECTIONS TO SCALING FOR THE HOLON MASS

In this appendix, we discuss the stability of the QCP. We will start by evaluating the diagram

$$\Pi_a^{(1)}(T) =$$

$$\Pi_a^{(1)}(T) = 2T^2 V^4 \sum_{n,m \neq 0} \sum_{\mathbf{k},\mathbf{q}} D_b(\mathbf{q}, \Omega_m)$$

$$\times G_c^2(\mathbf{k}, \omega_n) G_f(\mathbf{k}, \omega_n) G_f(\mathbf{k}+\mathbf{q}, \omega_n + \Omega_m).$$

Introducing the angle θ defined by $\epsilon_{\mathbf{k}+\mathbf{q}} = \epsilon_\mathbf{k} + v_F q \cos \theta$ and considering linearized bands such as in Eq. (A1), we have, with $\bar{g} = 8k_F^2 V^2/\rho_0$,

$$\Pi_a^{(1)}(T) = \bar{g}\rho_0 T^2 \sum_{n,m \neq 0} \sum_{\mathbf{q}} \int d\theta d\epsilon \frac{1}{q^2 + \frac{\gamma|\Omega_m|}{\alpha' q}}$$

$$\times \frac{1}{(i\omega_n - \epsilon + \mu)^2} \frac{1}{(i\omega_n - \alpha'\epsilon - \epsilon_f)}$$

$$\times \frac{1}{(i\omega_n + i\Omega_m - \alpha'\epsilon - \alpha' v_F q \cos \theta - \epsilon_f)}.$$

Summing over the fermionic Matsubara frequencies ω_n then integrating over ϵ, we get

$$\Pi_a^{(1)} = \bar{g}\rho_0 \alpha' T \sum_{\mathbf{q},m \neq 0} \int d\theta \frac{i\Omega_m}{q^2 + \frac{\gamma|\Omega_m|}{\alpha' q}} \frac{1}{i\Omega_m - \alpha' v_F q \cos \theta}$$

$$\times \frac{1}{i\alpha'\Omega_m - \alpha' v_F q \cos \theta - \alpha'\mu - \epsilon_f}$$

$$\times \frac{1}{i\Omega_m - \alpha' v_F q \cos \theta - \alpha'\mu - \epsilon_f}.$$

Now, we have $\mathbf{q} = (q_x, q_y)$ with $q_x = \cos \theta$ and $q_y = q \sin \theta$. We suppose $q_y \gg q_x$ and expand $q = \sqrt{q_x^2 + q_y^2} \simeq |q_y| + q_x^2/(2|q_y|)$. We find

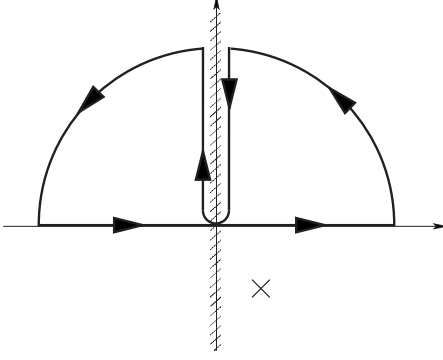FIG. 14. Contour of integration: the cross stands for a pole and the hatched line for a branch cut.

$$\Pi_a^{(1)}(T) = \frac{\bar{g}\rho_0\alpha'}{4\pi^2}T\sum_{m\neq 0}\int dq_x\int_{|q_x|}^{\Lambda}dq_y\frac{i\alpha'\Omega_m}{\gamma|\Omega_m|}$$

$$\times\frac{(|q_y|+q_x^2/(2|q_y|))}{i\Omega_m-\alpha'v_Fq_x}\times\frac{1}{i\alpha'\Omega_m-\alpha'v_Fq_x-\alpha'\mu-\epsilon_f}$$

$$\times\frac{1}{i\Omega_m-\alpha'v_Fq_x-\alpha'\mu-\epsilon_f},$$

where Λ is an ultraviolet cutoff.

A logarithmic singularity in q_x arises when we integrate over q_y and keeping only this singular part, we write

$$\Pi_a^{(1)}\sim\frac{\bar{g}\rho_0\alpha'}{8\pi^2}T\sum_{m\neq 0}\frac{i\alpha'\Omega_m}{\gamma|\Omega_m|}\int dq_x\frac{q_x^2\log(\Lambda/|q_x|)}{(i\Omega_m-\alpha'v_Fq_x)^3}.$$

$\Pi_a^{(1)}$ is performed by continuation in the upper half plane if $\Omega_m\leq 0$ and in the lower half plane if $\Omega_m\geq 0$ so that to avoid the pole in Green's function (see Fig. 14).

Changing variables in $q_x=iz$ we get

$$\Pi_a^{(1)}=-\frac{\bar{g}\rho_0\alpha'}{8\pi^2}T\sum_{m\neq 0}\frac{i\alpha'\Omega_m}{\gamma|\Omega_m|}\int_0^{\Lambda}idz\,\mathrm{sgn}(\Omega_m)$$

$$\times\frac{(-iz)^2[\log(-iz)-\log(iz)]}{(-i)^3(|\Omega_m|+\alpha'v_Fz)^3}$$

$$=-\frac{\bar{g}\rho_0\alpha'}{8\pi^2}T\sum_{m\neq 0}\frac{i\alpha'\Omega_m}{\gamma|\Omega_m|}\frac{i\pi\,\mathrm{sgn}(\Omega_m)}{(\alpha'v_F)^3}\log\left(\frac{\Lambda}{|\Omega_m|}\right).$$

To perform the summation over m, we notice that $T\sum_{-\Lambda/T}^{\Lambda/T}1=2\Lambda$ is independent of T. The same sum without the $m=0$ term will be $2\Lambda-T$ and to logarithmic accuracy, we obtain

$$T\sum_{m\neq 0}\log\left(\frac{\Lambda}{|\Omega_m|}\right)=-T\log\left(\frac{\Lambda}{T}\right)+\cdots,$$

where the dots stand for $O(T)$ terms.

Finally,

$$\Pi_a^{(1)}(T)=-\frac{V^2}{8\alpha'D^2}T\log\left(\frac{\Lambda}{T}\right). \tag{B1}$$

This term is of negative sign and dominant compared to E^*, thus it can destabilize the regime. It therefore puts the inter-
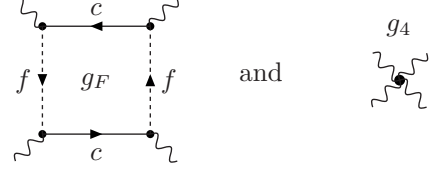

FIG. 15. The fermionic loop and the g_4 vertex.

mediate regime in a fragile situation. This is due to the presence of the fermion loop g_F (Fig. 15).

Fortunately, in $D=2$, a mode-mode coupling constant g_4, coming for example from the term $-Jn_in_j/4$ in Eq. (5), provides corrections to scaling of the same temperature dependence but with a positive sign $-T\log T$, competing with the one calculated previously. Indeed, for $g_4\geq 0$, the ϕ^4 theory is stable and, close to a QCP, the corrections to scaling follow the law[33]

$$m_b(T) = \quad g_4 \quad \sim T^{(d+z-2)/z}.$$

Precisely, the leading logarithmic contribution coming from the g_4 vertex reads

$$m_b(T)=\frac{g_4D_0}{6\pi}T\log\left(\frac{1}{T}\right)=g_4\frac{2D}{3V^2}T\log\left(\frac{1}{T}\right). \tag{B2}$$

The stability of the intermediate regime is then a matter of prefactors between the two terms. It can lie on a fragile basis as it requires strong enough ferromagnetic short-range fluctuations. However, it has been shown that this regime is stable for $D=3$.[14] We can thus expect that a small three-dimensional character could cure this instability. The correction to the boson mass coming from the gauge fluctuation
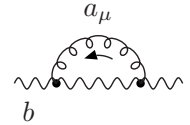
goes like T^2 in $D=2$ and are subdominant.[14]

APPENDIX C: EXPRESSION FOR THE FREE ENERGY

We start with the Luttinger-Ward formula (31). F_{MF} is the sum of the free energies of the two bands given by

$$F_{\mathrm{MF}}=-T\sum_{\pm}2\pi\rho_{\pm}\sum_n|\omega_n|.$$

The sum over the fermionic Matsubara frequencies is formally divergent but its temperature dependence can be extracted using the following spectral representation:

$$|\omega_n|=-\frac{1}{\pi}\int\frac{xdx}{x-i\omega_n},$$

then, performing the summation over Matsubara frequencies, with

$$T\sum_n \frac{1}{x - i\omega_n} = \frac{1}{2} - n_F(\omega_n),$$

we get

$$T\sum_n |\omega_n| \to \frac{\pi T^2}{6}.$$

We turn now to the bosonic part of Eq. (31)

$$F_h = \frac{T}{2}\sum_m \int \frac{dq^2}{(2\pi)^2} \log[D^{-1}(\mathbf{q}, \Omega_m)]$$

$$= \frac{T}{4\pi}\sum_m \int_0^{+\infty} q\,dq\,\log\left[q^2 + \xi^{-2} + \frac{\gamma|\Omega_m|}{\alpha' q} \right].$$

The integral over the holon momentum is dominated by large momenta and we have

$$F_h \approx \frac{T}{4\pi}\sum_m \int_0^{+\infty} \frac{\gamma|\Omega_m|}{\alpha' q(q^2 + \xi^{-2})} = \frac{\gamma\xi}{8\alpha'}T\sum_m |\Omega_m|.$$

Summation over the bosonic Matsubara frequencies is performed in the same way as for the sum over fermionic frequencies, and we find, for the T-dependent part of it,

$$T\sum_m |\Omega_m| \to -\frac{\pi T^2}{3}.$$

We end up with the total free energy given by

$$F = -\frac{\pi T^2}{6}\left[2\pi(\rho_+ + \rho_-) + \frac{\gamma\xi}{4\alpha'} \right]. \qquad (C1)$$

[1] G. Stewart, Rev. Mod. Phys. **56**, 755 (1984); **73**, 797 (2001).

[2] H. v. Löhneysen, Achim Rosch, Matthias Vojta, and Peter Wölfle, Rev. Mod. Phys. **79**, 1015 (2007).

[3] P. Coleman, C. Pépin, Q. Si, and R. Ramazashvili, J. Phys.: Condens. Matter **13**, R723 (2001).

[4] A. Rosch, A. Schröder, O. Stockert, and H. v. Löhneysen, Phys. Rev. Lett. **79**, 159 (1997); A. Rosch, *ibid.* **82**, 4280 (1999).

[5] M. Neumann, Ján Nyéki, Brian Cowan, and John Saunders, Science **317**, 1356 (2007).

[6] H. Franco, R. E. Rapp, and H. Godfrin, Phys. Rev. Lett. **57**, 1161 (1986).

[7] D. S. Greywall, Phys. Rev. B **41**, 1842 (1990).

[8] E. Collin, S. Triqueneaux, R. Harakaly, M. Roger, C. Bauerle, Y. M. Bunkov, and H. Godfrin, Phys. Rev. Lett. **86**, 2447 (2001).

[9] K. D. Morhard, C. Bauerle, J. Bossy, Y. Bunkov, S. N. Fisher, and H. Godfrin, Phys. Rev. B **53**, 2658 (1996).

[10] M. Roger, Phys. Rev. Lett. **64**, 297 (1990).

[11] G. Misguich, B. Bernu, C. Lhuillier, and C. Waldtmann, Phys. Rev. Lett. **81**, 1098 (1998).

[12] A. Benlagra and C. Pépin, Phys. Rev. Lett. **100**, 176401 (2008).

[13] I. Paul, C. Pépin, and M. R. Norman, Phys. Rev. Lett. **98**, 026402 (2007).

[14] C. Pépin, Phys. Rev. B **77**, 245129 (2008).

[15] C. Pépin, Phys. Rev. Lett. **98**, 206401 (2007).

[16] D. Vollhardt, Rev. Mod. Phys. **56**, 99 (1984).

[17] M. Héritier, J. Phys. (Paris), Lett. **40**, L451 (1979).

[18] M. Roger, C. Bäuerle, H. Godfrin, L. Godfrin, and J. Treiner, J. Low Temp. Phys. **112**, 451 (1998).

[19] P. Coleman, Phys. Rev. B **29**, 3035 (1984).

[20] L. Pricaupenko and J. Treiner, Phys. Rev. Lett. **72**, 2215 (1994).

[21] S. Tasaki, Prog. Theor. Phys. **79**, 1311 (1988).

[22] A. Hewson, *The Kondo Problem to Heavy Fermions* (Cambridge University Press, New York, 1997) p. 333.

[23] The fitting of the data with the three parameters depends mainly on adjusting the hybridization and is very robust to a change in the initial condition, which can always be accounted by a rectification of the parameters V_1 and V_2. Taking into account the self-consistent determination of b changes very slightly the result of Ref. 12 and the phase diagram is essentially the same.

[24] T. Senthil, Matthias Vojta, and Subir Sachdev, Phys. Rev. B **69**, 035111 (2004).

[25] S. Burdin, A. Georges, and D. R. Grempel, Phys. Rev. Lett. **85**, 1048 (2000).

[26] P. Nozières, Ann. Phys. (Paris) **10**, 19 (1985); Eur. Phys. J. B **6**, 447 (1998).

[27] I. Paul, C. Pépin, and M. R. Norman, Phys. Rev. B **78**, 035109 (2008).

[28] A dynamical exponent z is defined as the number of space dimensions that are effectively taken by the quantum fluctuations, namely, $\omega \sim q^z$.

[29] D. Belitz, T. R. Kirkpatrick, and T. Vojta, Phys. Rev. B **55**, 9452 (1997).

[30] A. V. Chubukov, D. L. Maslov, S. Gangadharaiah, and L. I. Glazman, Phys. Rev. B **71**, 205112 (2005).

[31] J. Rech, C. Pépin, and A. V. Chubukov, Phys. Rev. B **74**, 195126 (2006).

[32] P. A. Lee, N. Nagaosa, and X.-G. Wen, Rev. Mod. Phys. **78**, 17 (2006).

[33] J. Zinn-Justin, *Quantum Field Theory and Critical Phenomena* (Oxford Science, New York, 2002).